Proceedings of the Canadian Society for Mechanical Engineering International Congress 2021
CSME Congress 2021
June 27-30, 2021, Charlottetown, PE, Canada

Flow Control in Low-Reynolds Flow Using Flexible Gurney Flap

B. Afra[1]*, A. Tarokh[1,2]
[1,*] Faculty of Science and Environmental Studies, Lakehead University, Thunder Bay, Canada
[2] Department of Mechanical Engineering, Lakehead University, Thunder Bay, Canada
* Email: bafra@lakeheadu.ca
atarokh@lakeheadu.ca

Abstract- The structure of the wake behind immersed bodies can be manipulated via either passive or active flow control methods. In this study, the effects of a flexible Gurney flap on the wake structure are investigated. The Gurney flap as a passive flow control does not require an extra source of energy and it proved its capability of modification of the wake structure in low Reynolds number. We analyze the flow characteristics for the case in which a flexible gurney flap has been attached to a circular cylinder and is under affected of incoming uniform flow at different Reynolds numbers. We implemented a new robust numerical method including Immersed Boundary lattice Boltzmann Methods to find the flow filed and boundary forces which is combined with Lattice Spring Model for simulation of flexible Gurney flap. In order to verify the numerical method, fluctuation of a filament attached to the cylinder in downstream has been compared in terms of the fluctuation's amplitude. The gurney flap has been found to enhance lift experienced over the immersed body due to high pressure region generated at downstream of the flap. Also, lift to drag ratio is studied for different bending stiffness and length of the flap. The results show that flexibility changes the projected area in the normal direction, altering drag force and wake structure at downstream of the whole structure.

Keywords-component; formatting; style; styling; insert (key words)

I. INTRODUCTION

The field of low-Reynolds number fluid structure interaction has extensively received consideration over the past decade due to the high range of applications, such as imitation of fishing motions for fabricating of soft robotics [1], heat transfer advancement using vortex generator flapping fins [2] and flow control of aerial vehicles suffers from stalls in high angle of attacks [3]. For these applications, in particular computational flow control of immersed body, understanding the effect of the lift force on the boundary edges of deformable becomes vital. On the other hand, drag forces play a paramount role in such problems as drags reduce kinetic energy of fluid flows in the vicinity of the structure.

Flow control study of immersed body undergoes a low-Reynolds number incoming fluid flow has been widely performed by different research groups, either passively [4, 5] and actively [6, 7]. Active control approaches require energy and usually are efficient in high Reynolds numbers to delay and remove stalls on aircrafts' wings. They are less-effective in very low Reynolds numbers (e.g., in order of 10^2 to 10^3) since passive flow control methods are as successful as active ones [8]. Active flow control methods operate when they are needed, and require control devices and actuators [8]. Thus, the problems in which lift and drag forces can be controlled passively are not reasonable to be combined by active flow control methods. In this study, hydrodynamic forces on the circular cylinder are studied to figure out how a simple, effective passive method, namely Gurney flap attachment, can optimize the flow structure at downstream of the flap.

The Gurney flap attached to the structure's boundaries are extensively seen in popular researches in the field of immersed bodies' flow control [9, 10]. Gurney flap consists of a thin plate vertically attached to the pressure-side of immersed bodies (particularly airfoils), resulting in an increment in lift coefficient. While drag coefficients will also increase by an extra device perpendicular to the stream-wise. In the previous studies [11, 12] showed that ratio of lift to drag coefficients (D_{LD}) may be larger than that of clean cylinder and differs by altering location of the flaps. There are extensive researches on Gurney flaps in the literature in high Reynolds number to examine effects of the flap's height and its location on generating higher lift-to-drag ratio [13-15]. However, the information about the effects of the flexible flap on the lift coefficient and the structure of wakes behind the immersed body is very limited. In this study, we simulate a circular cylinder equipped by a flexible Gurney flap and determined the effects of its flexibility, size and configuration on the lift-to-drag ratio and flow behavior behind the cylinder.

II. ON THE COMPUTATIONAL APPROACH

A. Lattice Boltzmann Method

To resolve momentum and continuity equations of incompressible fluid flows based on Lattice Boltzmann Method, it can be written [16]:

$$f_i\left(\vec{r}+\vec{e_i}\delta t, t+\delta t\right)= f_i\left(\vec{r},t\right)- \tau^{-1}\left[f_i\left(\vec{r},t\right)- f_i^{eq}\left(\vec{r},t\right)\right] \quad (1)$$

Where f_i denotes distribution function in each direction in spatial position $\vec{r}$ and time t. Also, equilibrium distribution function gets the form as follow:

$$f_i^{eq} = w_i\rho\times \left[1+\frac{3}{c^2}\left(\vec{e_i}.\vec{u}\right)+\frac{9}{2c^4}\left(\vec{e_i}.\vec{u}\right)^2-\frac{3}{2c^2}\vec{u}.\vec{u}\right] \quad (2)$$

where $w_{1-4}=\frac{1}{9}$, $w_{5-8}=\frac{1}{36}$ and $w_0=\frac{4}{9}$ If D_2Q_9 is considered for LB [16], discrete velocity vector is defined as follow:

$$\vec{e_i} = c\begin{bmatrix}1 & 0 & -1 & 0 & 1 & -1 & -1 & 1 & 0\\ 0 & 1 & 0 & -1 & 1 & 1 & -1 & -1 & 0\end{bmatrix} \quad (3)$$

Where $c=\delta x/\delta t$. LBM is divided to two steps, including collision and streaming. The collision method is resolved with Eqs (1-3) and streaming method is recovered by moving of each towards their neighbors. Thus, density and velocity of the fluid flow in each position $\vec{r}$ and time t are introduced:

$$\rho=\sum_i f_i=\sum_i f_i^{eq} \qquad \rho\vec{u}=\sum_i \vec{e}_i f_i+\frac{\delta t}{2}\vec{F} \quad (4)$$

Also, based on Chapman-Enskog theory [17], kinematic viscosity gets the form as follow:

$$\nu = c_s^2\left(\tau-\frac{1}{2}\right)\delta t \quad (5)$$

where τ is single relaxation time and plays an important role in converting macroscopic properties to meso-scale Lattice Boltzmann parameters. c_s is the speed of sound takes the value of $1/\sqrt{3}$ for this model.

B. Immersed Boundary-Lattice Spring Method

In fluid-structure interaction problem, an external body force is added to the LB equations as follow [18]:

$$f_i\left(\vec{r}+\vec{e_i}\delta t, t+\delta t\right)= f_i\left(\vec{r},t\right)- \tau^{-1}\left[f_i\left(\vec{r},t\right)- f_i^{eq}\left(\vec{r},t\right)\right]+F_i\left(\vec{r},t\right)\delta t \quad (6)$$

Where

$$F_i\left(\vec{r},t\right)=\left(1-\frac{1}{2\tau}\right)w_i\times \left[3\frac{\vec{e_i}-\vec{u}\left(\vec{r},t\right)}{c^2}+9\frac{\vec{e_i}.\vec{u}\left(\vec{r},t\right)}{c^4}\vec{e_i}\right].\vec{F}\left(\vec{r},t\right) \quad (7)$$

Based on Immersed-Boundary Method, the boundary force $\vec{F}\left(\vec{r},t\right)$ is obtained [18]:

$$\vec{F}\left(\vec{r}_b,t+\delta t\right)=\rho\frac{\vec{U}_b^{\,desire}-\vec{u}_b^{\,nof}\left(\vec{r}_b,t+\delta t\right)}{\delta t/2} \quad (8)$$

where $\vec{U}_b^{\,desire}$ is the velocity at the boundary point *b* and $\vec{u}_b^{\,nof}$ is defined as no-forced velocity and is give as:

$$\vec{u}_b^{\,nof}=\sum_{b=1}^{n}\vec{u}^{nof}\left(\vec{r}_{ij},t\right)D\left(\vec{r}_{ij}-\vec{r}_b\right) \quad (9)$$

where subscripts *i, j* demonstrate Eulerian grid points in horizontal and vertical directions and *D* is the Dirac delta function for interpolation of Eulerian velocities on each Lagrangian nodes.

In order to simulate deformation of Gurney flaps undergo deformation due to the hydrodynamic forces, implicit Lattice Spring Model (LSM) is employed as [16]:

$$E_s=\sum_{i=1}^{4}\frac{1}{2}k_n\left(\vec{r}_{ij}-\vec{r}_n^{\,eq}\right)^2+ \sum_{i=5}^{8}\frac{1}{2}k_{n-n}\left(\vec{r}_{ij}-\vec{r}_{n-n}^{\,eq}\right)^2 \quad (10)$$

where $\vec{r}_n^{\,eq}$ and $\vec{r}_{n-n}^{\,eq}$ are, respectively, the force-free length of nearest and the next nearest links connected to node *j*. Also, k_n k_n and k_{n-n} are respectively, the spring constants in nearest and nest-nearest direction. The next and next-nearest direction denote direct and diagonal neighbors. The Young modulus of elasticity, E_Y, can be found as:

$$E_Y = \frac{8k_n}{3} \tag{11}$$

$$k_n = \frac{k_{n-n}}{2} \tag{12}$$

If assume fluid forces are the only external force on the Gurney flap, the structure's configuration is updated in each time step as our robust implicit LSM [16]:

$$\vec{r}_i = \frac{1}{4}\Big(\frac{\vec{F}_{ij}^{ext}}{k_n + k_{n-n}} + \frac{k_n}{k_n + k_{n-n}} \sum_{j=1}^{4} \frac{a_0}{|\vec{r}_{ij}|}\vec{r}_{ij} + \frac{k_{n-n}}{k_n + k_{n-n}} \sum_{j=5}^{8} \frac{\sqrt{2}a_0}{|\vec{r}_{ij}|}\vec{r}_{ij} \tag{13}$$

where original length of nearest and next-nearest bonds are a_0 and $\sqrt{2}a_0$, respectively. Due to implicit nature of the proposed scheme, the computational cost increases; however, there is no restriction on the range of lattice size.

III. RESULTS

In this section, outcomes achieved for flow over a circular cylinder equipped with and without the Gurney flap that attached to the bottom surface (Fig. 1). Altering the flap height (h/D), flexibility $Ca = E_Y / \rho_f U^2$ and its angle (α) bring about various changes to the drag $C_D = F_x / \rho_f U^2 D$ and lift $C_L = F_y / \rho_f U^2 D$ coefficients over the immersed structure.

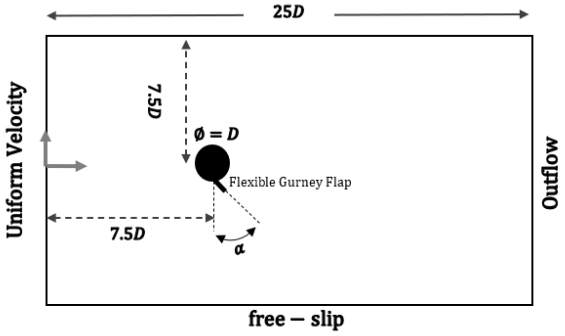

Fig.1. Schematic diagram of flexible Gurney flap attached to a fixed cylinder and undergoing a uniform flow

First, the simulation of flow over a fixed circular cylinder is carried out in Reynolds number of $\mathrm{Re} = UD/\nu = 100$ and angle of $\alpha = \pi/2$ and $Ca = 1400$. As indicated by Tian et. al [19], drag coefficient and fluctuation amplitude of the flap tip (δ_t / D) respectively get the values of *4.11* and 0.78. In this case, density ratio is $\rho_s / \rho_f = 10$. where ρ_s, ρ_f and ν denote the flap density, fluid flow density and kinematic viscosity of the fluid respectively. Table1 shows the values of the drag coefficient for different number of lattices. The value of the drag coefficient for the domain with 600×1200 lattices is in a close agreement with the results of Tian et. al [19].

Table1. Grid study on the drag coefficient over the cylinder equipped with a straight flexible flap.

Grid-study	**Present**			
	200×400	400 × 800	600 × 1200	800 × 1600
C_D	4.32	4.18	4.08	4.06
δ_t / D	0.89	0.82	0.79	0.78

For simulation of the flap's effects on drag and lift coefficients, the third force-related coefficient is defined as a ratio of lift to drag coefficients $D_{LD} = C_L / C_D$.

In the case of Gurney flap is vertically attached to the cylinder, to have a better understanding in the flap effects on structure, it is reasonable to modify drag and lift coefficients as follow:

$$C_D = F_x / \rho_f U^2 L_P \tag{14}$$

$$C_L = F_y / \rho_f U^2 L_P \tag{15}$$

where $L_p = D + h$, h demonstrates the flap length.

A. *Investigation of the flap length on the lift-to-drag ratio*

In this section, we examine how the vertical length of a rigid flap plays an important role in unsteady forces induced on the immersed structure. Fig.2 shows variation of D_{LD} in terms of h. As it is shown in Fig. 2, the length of Gurney flap has significant effects in lift-to-drag ratio. In fact, by increasing *L/D* to the value of 0.2, the average of D_{LD} increases sharply to the maximum value of 0.33. Afterwards, length increment no longer change the average of lift-to-drag and even reduces the ratio in lengths of 0.42 and 0.5. As it is expected, Gurney flaps are efficient in a particular range of *L/D*. Note that, the clean cylinder has been shown by *L/D* of zero in which gets the minimum value.

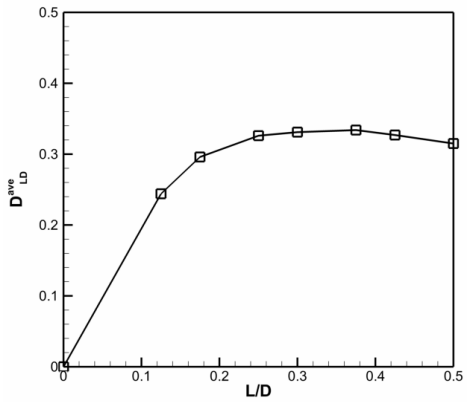

Fig.2. Variation of average lift-to-drag coefficient D_{LD}^{ave} in term of Gurney flap's length *(L/D).*

Fig.3 illustrates temporal variation of D_{LD} in different lengths of Gurney flap. As show, both amplitudes and maximum values of fluctuations in Gurney-equipped cylinders are by the far bigger than those of clean cylinder.

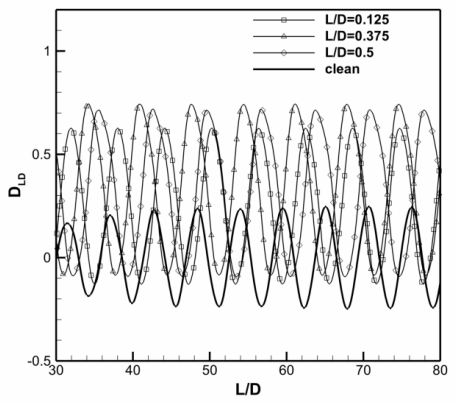

Fig.3. Temporal variation of D_{LD} in three different lengths of Gurney flap compared to the clean cylinder where there is no Gurney flap.

B. *The effect of the Gurney flap angle (α) on D_{LD}*

It is found that for the same lengths Gurney flaps but different angles α (see Fig.1), the lift-to-drag ratio varied, significantly. It is worth mentioning that the variation in angles can help to understand how important is relocating the stagnation point in control flows of swimmers. In fact, we could change the upstream, high-pressure region around the cylinder by altering the angle of flap. In order to have a comprehensive understanding of the effects of the angles, a Gurney flap is attached to the cylinder bottom, ranging -90, -60, -45, -30, -20, 0, 20, 30, 45, 60 and 90 degrees. Fig. 4 shows the average lift-to-drag ratio as a function of α for a flap with the length L/D=0.375. We have observed that the case with α=45° gets the maximum D_{LD} of 0.42 even more than that of the vertical flap. Also, the horizontal flap α=-90° changes formation of the pressure field so that minimum lift is achieved. Fig.5 proves the temporal fluctuations of D_{LD} in different angles. It is clear that α=45° generates the biggest D_{LD}^{ave} and $\left|D_{LD}^{ave}\right|$.

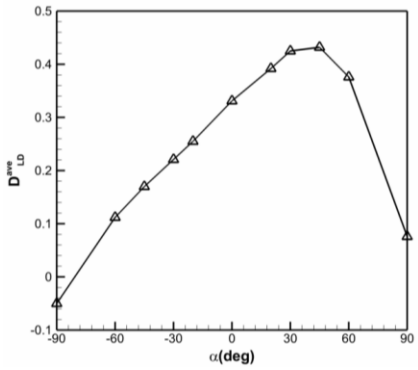

Fig. 4. Variation of average lift-to-drag coefficient D_{LD}^{ave} in term of α

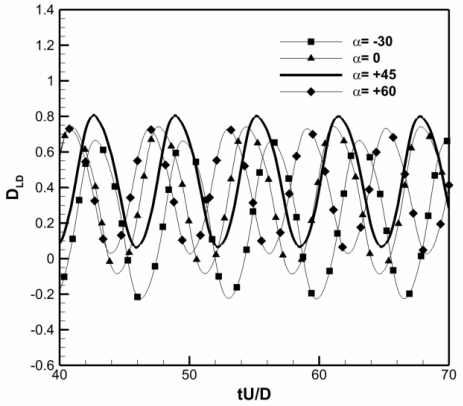

Fig.5. Temporal variation of D_{LD} in three different angles of -30, +45 and +60 degree compared to vertical one. The length of the flap (L/D) is 0.375

Fig. 6 explains why positive angles of attack induce efficient flow regimes in the vicinity of the cylinder so that lift-to drag ratio increases compared to the vertical one. Pressure

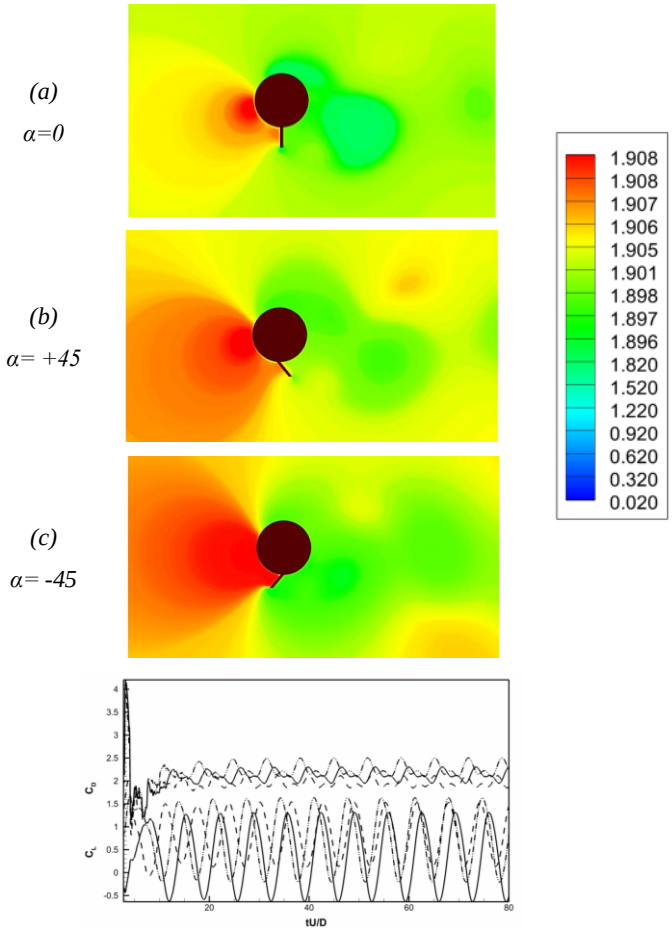

Fig.6. a-c: Pressure distribution of fluid flow around the structure. d: drag and lift coefficients on the structure for different angles of Gurney flap. Solid, dashed and dashed-dot-dot lines respectively denote α=-45°, 0° and 45°.

distribution of fluid flow has been shown in Fig. 6. Comparing drag and lift coefficient with pressure contours, we found that lift forces significantly decreased as α decreases from positive values to negative ones. This is because high pressure region

is stretched in the direction of the flap tip moves. In fact, the bigger α is, the stronger that part of the boundary under the influence of higher-pressure is. However, for α>60, the flap starts to help fluid flow to damp fluctuations, because stream-wise length of the flap exceeds than the perpendicular length, resulting in a larger wake behind the cylinder. It then progressively reduces the oscillation in down-stream [20] .

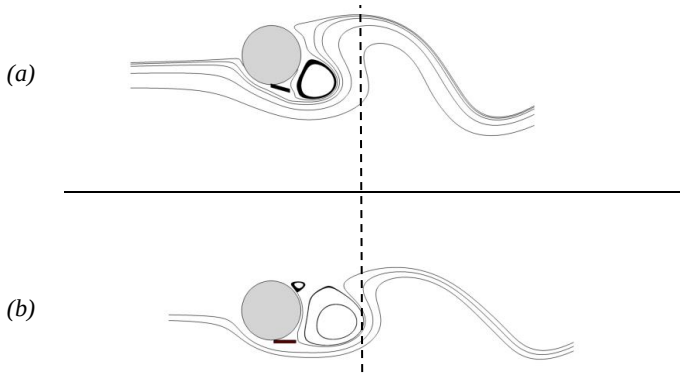

Fig.7 streamline demonstration of upcoming flows pass over the structure when (a) α is 60° and (b) α is 90°.

C. *Investigation the effect of* Ca *in altering* D_{LD}

In real applications, Gurney flaps undergo deformation which influence flow regieme in the vicinity of the flap. Thus, in this section the flap can freely moves or even fluctuate under the applied hydrodynamic forces from the flow. The capillary number is varied in order to study the effects of flexibility on the lift-to-drag ratio.

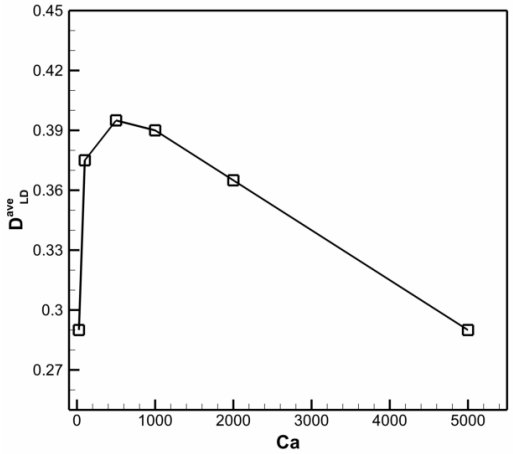

Fig. 8. Effects of Capillary number on the lift-to-drag ratio

Fig. 8 shows that the flexible flap compared to the rigid one induces greater D_{LD}. It is also obtained that *Ca* of *500* leads to the different formation in which the lift force gets the maximum value of *0.4*. Fig. 9 demonstrates that stiffer Gurney flaps vibrate with higher amplitudes while flexible ones undero larger deformations (δ/D) without any fluctuations. As depicted in Fig. 9, filaments with *Ca* of *25* and *100* cause the whole structure to be more aerodynamic and decrease the fluctuations in downstream, just like what has happened in the rigid flap with the angle of 90°. Thus, the flap flexibility successfully optimize the current flow-control mechanism, except the conditions cause large deformations and keep the flap very close to the surface. Although more aerodynamics configuration makes smaller drag (Fig. 9a), its weak fluctuation of lift force is not so strong that exceeds that of stiffer one (Fig. 9b).

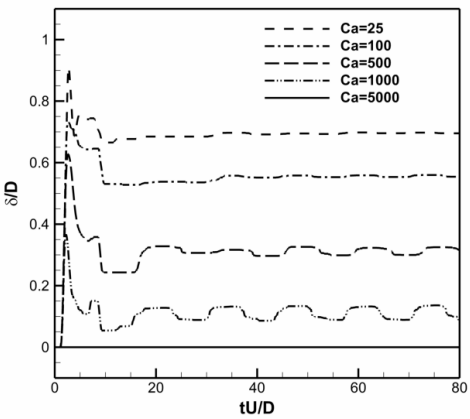

Fig. 8. Horizontal displacement of the flap in different Capillary numbers

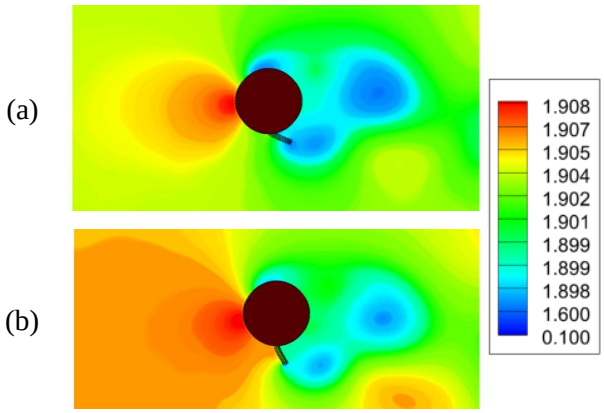

Fig. 9. Pressure distribution of the flow in the vicinity of the structure in *(a) Ca=25 and (b) Ca=500*

IV. CONCLUSION

In this study, hydrodynamics effects of a Gurney flap attached to the cylinder boundary has been investigated. Immersed Boundary Lattice Boltzmann Method along with Lattice Spring Model have been employed to determine fluid structure interaction forces that cause deformation in the flap. Analyzing the lift spectra and flow structure of the wake in different Gurney flap's length reveals that there is a maximum size for the flap to make the most efficient structure. Also, the angle of flap with vertical axis may cause more lift forces compared to the typical angle of zero. It has been proved here a 45° counter-clock wise deviation from the vertical axis makes the most efficient configuration. And finally, the results suggest that flexible filaments are successful to enhance lift-to-drag coefficient compared to the rigid one.

References

[1] A. Hess, X. Tan, and T. Gao, "CFD-based multi-objective controller optimization for soft robotic fish with muscle-like actuation," Bioinspiration & biomimetics, vol. 15, p. 035004, 2020.

[2] R. K. B. Gallegos and R. N. Sharma, "Flags as vortex generators for heat transfer enhancement: Gaps and challenges," Renewable and Sustainable energy reviews, vol. 76, pp. 950-962, 2017.

[3] J. A. Witteveen, S. Sarkar, and H. Bijl, "Modeling physical uncertainties in dynamic stall induced fluid–structure interaction of turbine blades using arbitrary polynomial chaos," Computers & structures, vol. 85, pp. 866-878, 2007.

[4] B. Afra, A. Amiri Delouei, M. Mostafavi, and A. Tarokh, "Fluid-structure interaction for the flexible filament's propulsion hanging in the free stream," Journal of Molecular Liquids, vol. 323, p. 114941, 2021/02/01/ 2021.

[5] P. Kundu, "Numerical simulation of the effects of passive flow control techniques on hydrodynamic performance improvement of the hydrofoil," Ocean Engineering, vol. 202, p. 107108, 2020.

[6] D. Velasco, O. L. Mejia, and S. Laín, "Numerical simulations of active flow control with synthetic jets in a Darrieus turbine," Renewable Energy, vol. 113, pp. 129-140, 2017.

[7] J. Li and X. Zhang, "Active flow control for supersonic aircraft: A novel hybrid synthetic jet actuator," Sensors and Actuators A: Physical, vol. 302, p. 111770, 2020.

[8] H. H. Ali and R. C. Fales, "A review of flow control methods," International Journal of Dynamics and Control, 2021/01/04 2021.

[9] Y. Liu, K. Li, J. Zhang, H. Wang, and L. Liu, "Numerical bifurcation analysis of static stall of airfoil and dynamic stall under unsteady perturbation," Communications in Nonlinear Science and Numerical Simulation, vol. 17, pp. 3427-3434, 2012.

[10] K. Menon and R. Mittal, "Aerodynamic Characteristics of Canonical Airfoils at Low Reynolds Numbers," AIAA Journal, vol. 58, pp. 977-980, 2020.

[11] H. Dumitrescu and I. Mălăel, "Analysis of low Reynolds number flow past Gurney flap," INCAS Bulletin, vol. 2, pp. 97-105, 2010.

[12] R. H. Liebeck, "Design of subsonic airfoils for high lift," Journal of aircraft, vol. 15, pp. 547-561, 1978.

[13] B. L. Storms and C. S. Jang, "Lift enhancement of an airfoil using a Gurney flap and vortex generators," Journal of Aircraft, vol. 31, pp. 542-547, 1994.

[14] J. Wang, Y. Li, and K.-S. Choi, "Gurney flap—Lift enhancement, mechanisms and applications," Progress in Aerospace Sciences, vol. 44, pp. 22-47, 2008.

[15] Y. Zhang, V. Ramdoss, Z. Saleem, X. Wang, G. Schepers, and C. Ferreira, "Effects of root Gurney flaps on the aerodynamic performance of a horizontal axis wind turbine," Energy, vol. 187, p. 115955, 2019.

[16] B. Afra, M. Nazari, M. Kayhani, A. A. Delouei, and G. Ahmadi, "An immersed boundary-lattice Boltzmann method combined with a robust lattice spring model for solving flow–structure interaction problems," Applied Mathematical Modelling, vol. 55, pp. 502-521, 2018.

[17] S. Wolfram, "Cellular automaton fluids 1: Basic theory," Journal of statistical physics, vol. 45, pp. 471-526, 1986.

[18] B. Afra, M. Nazari, M. H. Kayhani, and G. Ahmadi, "Direct numerical simulation of freely falling particles by hybrid immersed boundary–Lattice Boltzmann–discrete element method," Particulate Science and Technology, 2019.

[19] F.-B. Tian, H. Dai, H. Luo, J. F. Doyle, and B. Rousseau, "Fluid–structure interaction involving large deformations: 3D simulations and applications to biological systems," Journal of computational physics, vol. 258, pp. 451-469, 2014.

[20] C. Apelt, G. West, and A. A. Szewczyk, "The effects of wake splitter plates on the flow past a circular cylinder in the range 104< R< 5× 104," Journal of Fluid Mechanics, vol. 61, pp. 187-198, 1973.

.